AOF LTAO mode: reconstruction strategy and first test results

Sylvain Oberti[a], Johann Kolb[a], Miska Le Louarn[a], Paolo La Penna[a], Pierre-Yves Madec[a], Benoit Neichel[b], Jean-François Sauvage[c], Thierry Fusco[b,c], Robert Donaldson[a], Christian Soenke[a], Marcos Suárez Valles[a], Robin Arsenault[a]

[a]European Southern Observatory,
Karl-Schwarzschild-Str. 2, 85748 Garching bei München, Germany
[b]Aix Marseille Université, CNRS, Laboratoire d'Astrophysique de Marseille UMR 7326, 13388 Marseille, France
[c]Office National d'Etude et de Recherche Aérospatiale
BP72 - 29 avenue de la Division Leclerc, 92322 Chatillon, France

ABSTRACT

GALACSI is the Adaptive Optics (AO) system serving the instrument MUSE in the framework of the Adaptive Optics Facility (AOF) project. Its Narrow Field Mode (NFM) is a Laser Tomography AO (LTAO) mode delivering high resolution in the visible across a small Field of View (FoV) of 7.5" diameter around the optical axis. From a reconstruction standpoint, GALACSI NFM intends to optimize the correction on axis by estimating the turbulence in volume via a tomographic process, then projecting the turbulence profile onto one single Deformable Mirror (DM) located in the pupil, close to the ground.

In this paper, the laser tomographic reconstruction process is described. Several methods (virtual DM, virtual layer projection) are studied, under the constraint of a single matrix vector multiplication. The pseudo-synthetic interaction matrix model and the LTAO reconstructor design are analysed. Moreover, the reconstruction parameter space is explored, in particular the regularization terms.

Furthermore, we present here the strategy to define the modal control basis and split the reconstruction between the Low Order (LO) loop and the High Order (HO) loop.

Finally, closed loop performance obtained with a 3D turbulence generator will be analysed with respect to the most relevant system parameters to be tuned.

Keywords: Adaptive Optics Facility, VLT, Deformable Secondary Mirror, Laser Tomographic Adaptive Optics, Wavefront Reconstruction, Regularization, Ground Layer Adaptive Optics, GALACSI Narrow Field Mode

1. INTRODUCTION

This paper is about the control strategy and more particularly the LTAO reconstruction scheme designed, tested and baselined for AOF's GALACSI NFM. After introducing the context of this work, we will overview the AOF's control strategy, highlighting the design of the tomography reconstructor. Then, we will present the results of the lab testing activities in Europe, focusing on the optimization of the regularization terms against turbulence and signal to noise ratio. Furthermore, the sensitivity of the reconstructor to mis-registration will be presented. Finally, we will anticipate the remaining work in the context of the VLT and ELTs.

2. CONTEXT OF THIS WORK

2.1 The AOF project

The AOF project will transform one ESO VLT Unitary Telescope into an adaptive telescope. This telescope (UT4 or Yepun) has been upgraded to accommodate the new components, is already equipped with four Laser Guide Star (LGS)

systems [1], and will receive a Deformable Secondary Mirror (DSM) at the end of 2016 [2]. In addition two AO wavefront sensing modules were built: GRAAL [3] for the HAWK-I infrared imager and GALACSI for the MUSE 3D spectrograph. In order to test those two modules in the controlled environment of a laboratory, the test bench ASSIST was designed to emulate an adaptive VLT including the Deformable Secondary Mirror, a star simulator and turbulence generator and a VLT focal plane re-imager [4].

In 2013 the DSM was mounted on top of ASSIST installed at ESO's Headquarters and was tested thanks to a special interferometric mode of the bench, allowing opto-electrical characterization of the 1170 actuators, flattening and measurement of the Influence Functions. For two years starting in February 2014, the two AO modules have undergone System Testing on ASSIST [5] (see Figure 1). This phase aimed at validating all the possible components and loops of the AO modules before installation at the actual VLT that comprises the added complexity of real LGSs, a harsher non-reproducible environment and the adaptive telescope control.

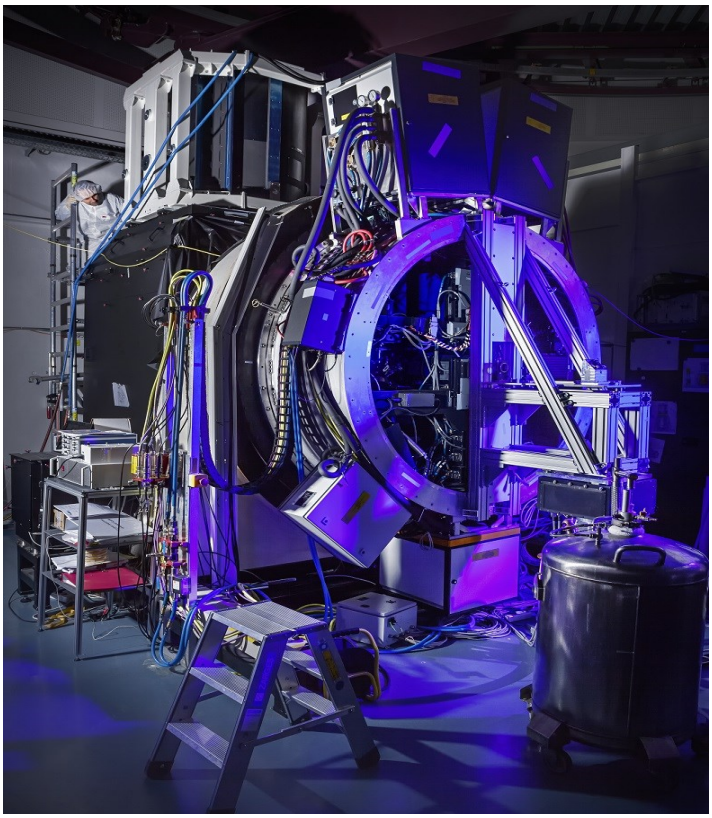

Figure 1: GALASCI AO module and the DSM mounted on the ASSIST test bench

2.2 GALACSI NFM for MUSE small FoV

GALACSI is the AO system serving the instrument MUSE in the framework of the AOF project. GALACSI offers two AO correction modes:

- The Wide Field Mode (WFM) is a Ground Layer AO (GLAO) mode delivering a homogeneous PSF across a FoV of 1' diameter. The results obtained during the WFM system tests are described in another paper at this conference [5] while the stand-alone testing is described in [6].
- The Narrow Field Mode (NFM) is a Laser Tomography AO (LTAO) mode delivering high resolution in the visible across a small FoV of 7.5" diameter around the optical axis. The specified performance is to achieve a Strehl Ratio (SR) of 5% (goal 10%) at 650 nm for a seeing of 0.65" with a Natural Guide Star (NGS) of magnitude 15 (goal: magnitude 16).

GALASCI NFM relies mostly on the same main subsystems as the WFM, i.e. the DSM with 1156 voice coil actuators in the pupil, 4 LGS Shack-Hartmann Wave Front Sensors (WFS) composed of 40x40 subapertures with 6x6 pixels of 0.8" read out at 1 kHz framerate. The main difference comes from the fact that GALACSI NFM makes use of a Low Order (LO) Natural Guide Star (NGS) loop correcting Tip/Tilt and Defocus thanks to an InfraRed (IR) 2x2 Shack-Hartmann WFS called IRLOS. IRLOS offers a large field acquisition mode and two scientific target guiding modes with a small plate scale (60 mas) and a large plate scale (250mas) to allow tracking extended objects. Two sampling frequencies are available: 208 Hz (baseline) and 500 Hz for bright objects.

The 4 LGS WFSs are co-rotating with the pupil (M2) such as to keep the LGSs in the WFS Field of View (FoV) and the DSM image clocking angle registered. IRLOS being located downstream MUSE's field derotator, the LO WFS commands are numerically rotated in order to match the DSM geometry at all angles.

3. CONTROL STRATEGY OVERVIEW

The AO control loop relies on the computation of a pseudo-synthetic reconstructor based on a numerical model tuned thanks to estimated and measured parameters. The main aspects of the control strategy are described in this section.

3.1 HO LGS and LO NGS loops

For every AOF LGS mode (GLAO and LTAO), the Tip/Tilt is fully controlled by the NGS LO loop. In the particular case of GALACSI NFM, the defocus is also measured by the NGS WFS. Two ways to control the defocus have been envisaged:

- Cascade control: The Defocus is controlled by a fast LGS loop (inner loop – f = 1 kHz), biased by Sodium layer altitude variation. A slower NGS loop (outer loop – f < 500 Hz), sends defocus offsets to the inner loop and act as the master loop removing the LGS biases.
- Orthogonal control: The Defocus is fully controlled by the NGS loop. The LGS loop control basis is orthogonal to Defocus.

The latter option has been selected as baseline for the sake of simplicity and because the fast defocus residuals showed to be negligible in the faint NGS case's error budget.

Finally Tip, Tilt and Defocus are fully controlled by the NGS LO loop. The HO LGS loop controls a modal basis based on Karhunen-Loeve modes, accounting for DSM influence functions and assuming a given atmospheric case (outer scale and Fried parameter). This modal basis is built to be orthogonal to the Tip, Tilt and Defocus modes. Finally, the theoretical projection of Tip, Tilt and Defocus on the LGS WFS slopes is subtracted from the measured slopes before reconstruction.

The Tip, Tilt and Defocus modes are defined as a trade-off between the amplitude of the force required to generate them and their optical quality resulting in fitting error. To perform this trade-off, the 3 modes are projected on the DSM stiffness modal basis ranked by increasing force (see Figure 2). For each mode, the maximum force is computed by multiplying the corresponding DSM position vector by the feed-forward matrix, converting a DSM command vector into force vector. On Figure 3, we can see that Tip-Tilt is almost fully generated with the first 10 stiffness modes and the required force is constant until ~600 modes and then slightly increasing, while Defocus requires modes around 100 to reach a reasonable fitting residual. Incidentally the use of those modes also increase the required force. Finally, 400 stiffness modes are selected to generate Tip-Tilt and 600 stiffness modes to generate Defocus, with an equivalent residual fitting error for the three modes as seen on Figure 4.

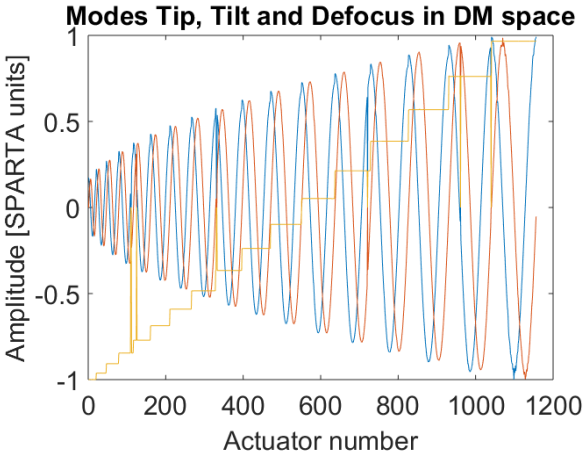

Figure 2: Modes Tip, Tilt and Defocus in DSM space after projection on influence functions. The disabled actuators are visible (amplitude=0)

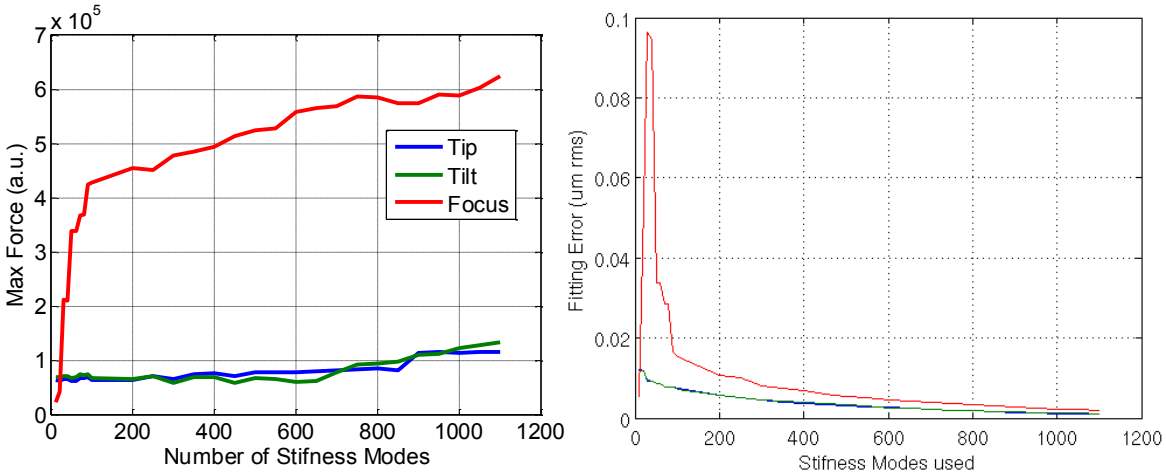

Figure 3: [Left] Max force required to produce Tip, Tilt and Defocus as function of the number of Stiffness modes used. [Right] fitting error.

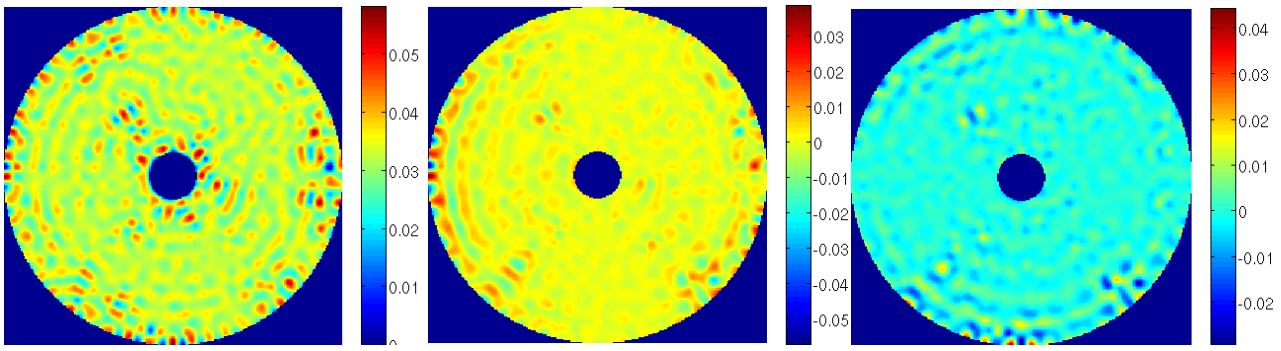

Figure 4: Fitting error after producing a 1 unit rms Tip with 400 Stiffness mode [Left], Tilt with 400 modes [Middle] or Focus with 600 modes [Right].

The interaction matrix between the LO modes and the NGS WFS is measured on sky. Two simple methods allow to measure the interaction matrix through turbulence:

- Fast push-pull in order to freeze and remove the atmosphere when subtracting push and pull signals [7], [8]

- Modulation of the modes and demodulation of the WFS measurements [8], [9]

The system tests have shown that the interaction matrix measured through turbulence was as good as the one measured on a calibration fiber, which will not be available once at the telescope.

3.2 Pseudo-Synthetic Interaction Matrix (PSIM)

To generate the HO interaction matrix, the AOF baseline is to compute a PSIM [10]. The term synthetic is used because the Interaction Matrix (IM) is generated via a numerical model. However, the parameters of the model are tuned with quantities measured on the real system. The main ingredients required to build the pseudo-synthetic interaction matrix are the following subsystem models:

- DSM model
- WFSs models
- Mis-registration between DSM and each LGS WFS lenslet array in terms of shift along the X and Y axes, rotation, magnification along the X and Y axes and pupil distortion if relevant.

Once these models are known (by design or through calibration) it is possible to synthetize the IM between the DM and the WFSs as illustrated in Figure 5. The PSIM approach is advantageous from several points of view:

- The PSIM can be noise-free if the input parameters are (Influence Functions in particular).
- They can be promptly re-generated and loaded when the optical configuration of the system changes, even while observing, provided that the configuration parameters are accurate.
- The PSIM update allows mitigating slow mis-registration which cannot be managed with a measured IM, such as pupil magnification, anamorphose and distortion
- Once the model of the system tuned during initial tests, the generation of the PSIM can be made free from daytime and even more importantly night-time calibrations, as opposed to what a measurement of IM through turbulence would do.

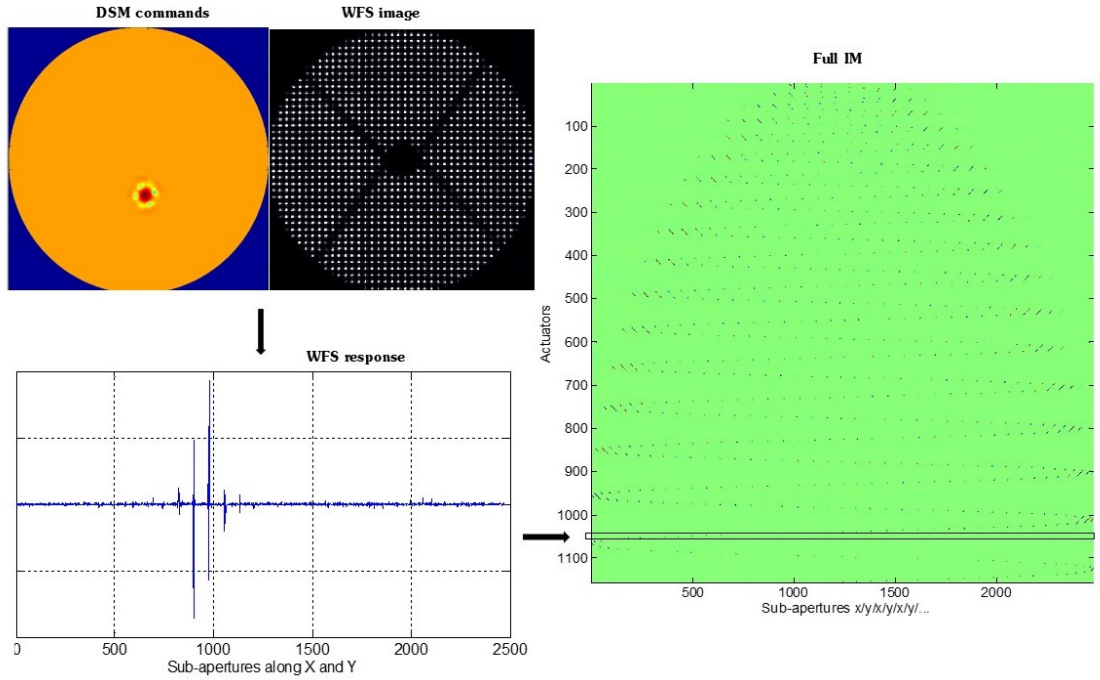

Figure 5: Pseudo-synthetic Interaction Matrix computation scheme - illustration of generation of a subset of the IM corresponding to the DSM as seen by one LGS WFS.

3.3 DSM model

The DSM is a position-driven DM controlled with a local voice coil servo loop. The influence functions are different from what we are used to. There is virtually no coupling between neighbor actuators because their position can be forced to 0. A Finite Element Analysis (FEA) of the thin shell was performed. It produced a set of synthetic influence functions, defined as the shape of the shell when one actuator is pushed to 1 micron while the others are forces to zero (see Figure 6). On ASSIST, the influence functions have been measured with an interferometer. They showed to be very close to the FEA model, except that some measurements were biased, noisy, or not exploitable because the actuator was partially hidden by the spiders. Thus, it has been decided to use the FEA influence functions as DM model for the PSIM computation. The amplitude of these influence functions is scaled in order to account for the fact that the measurement from the capacitive position sensor is integrated over a certain surface. Finally, the DSM model integrates the fact that disabled actuators (high resistance, oscillation) are slaved to their neighbors.

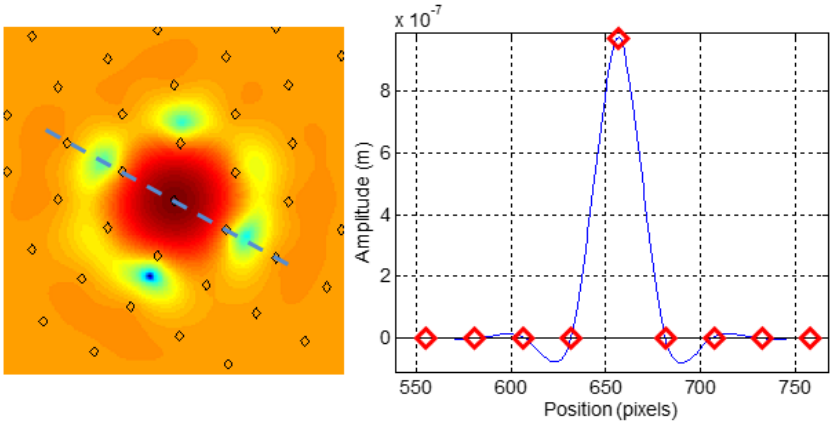

Figure 6: [Left] Example of a DSM Influence Function, the actuators positions are marked by diamonds. [Right] cross-cut of the left image (along the blue dotted line). The actuators positions are marked by red diamonds.

3.4 WFS model

The LGS WFSs Shack-Hartmann model is implemented in the PSIM code with different levels of complexity, up to a full diffractive model with noise, detector biases and non linearities. The tests on ASSIST have shown that a simple geometrical model was sufficient to describe the WFS accurately. This model takes the pupil shape into account but assumes a homogeneous slope response. In practice, different LGS spot elongations across the pupil and non-zero reference slopes induce a non-uniform slope response across the subapertures. These effects can be treated by multiplying the PSIM by a vector of slope response identified online. For AOF, this can be done by the LGS spot monitor [11] which records the spot dimensions in each subaperture. This information is also used to tune the weighted center of gravity online.

A dithering method could also be used to determine the slope response online. For example the LGS jitter mirrors could be modulated with a small amplitude without degrading the correction on the science path [12].

3.5 Mis-registration identification

To estimate mis-registration the pupil flux balance method (successfully implemented in SPHERE) is used on AOF for bootstrapping, but it provides only X/Y shifts, not rotation nor magnification, anamorphose or pupil distortion. For the AOF the adopted approach is to combine sets of real-time data (slopes and DSM commands, measured in closed loop without adding any disturbance to the system besides the turbulence itself) with the knowledge of the currently used IM in order to retrieve the shifts, rotation… and update the CM. It consists in generating one perfectly aligned PSIM and several “delta” IMs, i.e. PSIMs with small known mis-alignments. If we consider:

1) The real IM to be a linear combination of the perfect IM (PSIM) and of the delta IMs. For small perturbations, the relation between the perturbed IM and its nominal value (PSIM) writes:

$$\mathrm{IM} = \mathrm{PSIM} + \alpha_{\mathrm{rot}} \times \delta\mathrm{IM}_{\mathrm{rot}} + \alpha_{\mathrm{Xshift}} \times \delta\mathrm{IM}_{\mathrm{Xshift}} + \alpha_{\mathrm{Yshift}} \times \delta\mathrm{IM}_{\mathrm{Yshift}} + \ldots \qquad (1)$$

2) The delta IMs to have been recorded (by measurement or simulation) in the linear range of the mis-registration, and
3) The mis-registration delta IMs to be uncorrelated,

Then the coefficients α_{rot} … can be computed by simple projection of the IM error (difference between the measured and the perfect IM) on the delta IMs:

$$\alpha_{rot} = \frac{\left\| (IM - PSIM) \times \delta IM_{rot} \right\|}{\left\| \delta IM_{rot} \right\|^2} \quad (2)$$

In practice the non-exactness of the assumptions above can be overcome by the use of several iterations. The starting point for each new iteration is a PSIM re-computed at the mis-registration parameters estimated at the previous iteration.
The measurement of a crude IM can be extracted from the correlation between WFS measurements and DM commands while in closed AO loop during scientific observation, and this without applying any disturbance on the DM in addition to the one correcting turbulence [13]. Such an IM will lack the Signal to Noise Ratio required to deliver proper performance if used in the system, but it contains largely enough information to track the evolution of the system properties, mis-registrations in particular. This method is based on the fact that the slopes measured at an iteration (*i*) are linked to the voltages applied at the same iteration by the Interaction Matrix:

$$S(i) = V(i) \times IM + Turbulence + Noise \quad (3)$$

The same is true between the increment of slopes and voltages, with the advantage to reduce the turbulence and noise contributions:

$$\begin{aligned} &\delta S(i) = S(i) - S(i-1) = \\ &\left[V(i) - V(i-1)\right] \times IM + \delta_{Turb} + \delta_{Noise} + \ldots = \delta V(i) \times IM + \delta_{Turb} + \delta_{Noise} + \ldots \end{aligned} \quad (4)$$

Both sides of the equation can be multiplied by the pseudo-inverse $\delta V(i)^+$ of $\delta V(i)$, obtained by truncated Singular Value Decomposition (tSVD):

$$IM = \delta V(i)^+ \times \delta S(i) + \ldots \quad (5)$$

The resulting IM is injected in (2) which allows to retrieve the mis-registration parameters and to build the corresponding PSIM in order to update the CM if required. On ASSIST, the mis-registration estimation from real-time data has shown to be better than 10% of a subaperture in shift. The mis-registration loop converges from 25% to within 12% of a sub-aperture in 1 iteration. It provides an update typically every 10 minutes, to be consolidated during commissioning. Indeed, the update rate could be increased if required, by considering a subset of the IM to estimate the mis-registrations.

3.6 AO control

The AOF Real Time Computer (RTC) called SPARTA provides the following real time control features:

- A single Matrix Vector Multiplication (MVM) which constraints the reconstruction design
- An IIR temporal controller of order 5 which is typically configured as a leaky integrator
- An Adaptive Vibration Control algorithm (AVC) acting on the NGS LO sensor control loop and allowing to cancel-out some vibrations peaks whose frequency is above the control bandwidth. The vibration is tracked in real time in terms of frequency, amplitude and phase. The plant model can be tracked as well. The correction is applied as a feedforward added to the DSM commands.
- DSM anti-windup echo is sent to SPARTA which results in skipping the full control frame for each occurrence of saturation in force

In addition, the instrument software and SPARTA provide secondary loops such as the offload of the DSM pattern to the telescope active optics slow actuators (telescope axes, hexapod, M1), the focus loop driving the focus compensator common to the 4 LGS WFSs and the truth sensor loop which makes use of the active optics Shack-Hartmann as an NGS truth sensor whose average slopes are sent as offsets to the LGS WFSs' reference slopes. More details on the AOF control strategy can be found in [14].

4. TOMOGRAPHIC RECONSTRUCTION FOR GALACSI NFM

This section describes the tomographic reconstruction strategy implemented and tested with GALACSI NFM.

4.1 AO system geometry

As a prerequisite to building the tomographic reconstructor, the geometry of the tomographic system (see Figure 7 left) has to be identified. The following parameters, assumed by design or measured [6] [5], are essential ingredients of the tomographic reconstructor:

- LGSs off-axis angles: 10”
- Sodium layer altitude: 90 km
- Geometrical orientation of each LGS footprint in the metapupil: determined by measurement of reconstructed altitude static wavefront
- Reconstructed layers number and altitude: the ASSIST test bench simulates a turbulence profile incorporating 3 layers. Simulations have shown that it was not worth investigating more than 2 reconstructed layers in this case. The optimal altitude of the higher is around 8km as shown in Figure 7 right.

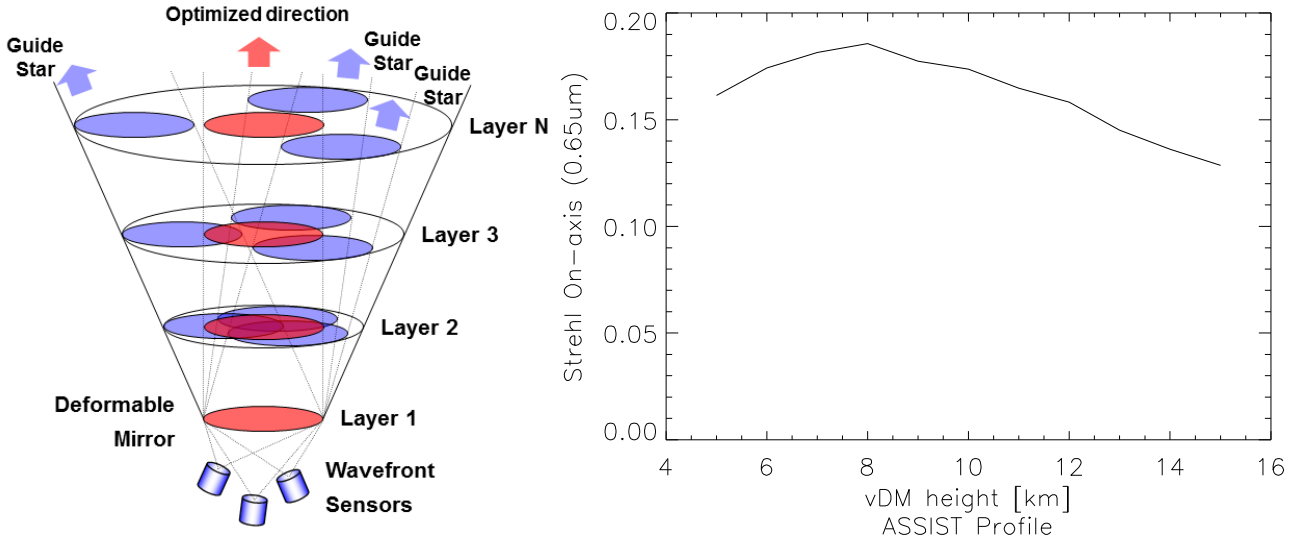

Figure 7: [Left] Illustration of the tomography geometry when using several GS in the FoV and optimizing the correction on axis [Right] End-to-End simulation with 3 layers turbulence profile: impact of reconstructed layer altitude on SR @ 650 nm

4.2 Computation of reconstructor: virtual DM method

The virtual DM (vDM) method consists in duplicating the ground DM (gDM) in altitude. This way, the central 8m disk in the metapupils is identical to the gDM, while the edges are zero padded. This minimalist model can perfectly describe the turbulence cylinder in the direction of optimization, the vDM being shifted according to the observing angle. It presents the advantage to be very easy to implement, as no projection is required to project the vDM shape onto the gDM, a basic sum of the commands being sufficient. Nevertheless, the edge of the metapupils not being modelled, the tomographic process is not taught how to deal with WFS signal resulting from the turbulence areas outside the on axis cylinder. Furthermore, edge effects must be taken-care of properly when building the vDM tomographic IM as described later. The main steps to build the vDM reconstructor are the following:

- Define a calibration modal basis for each DM. Even if different cases have been investigated (zonal, Zernike, Stiffness modes), in this study we select as modal basis for each DM the truncated DSM KL basis. The first NKL_{modes} modes are used to calibrate the following interaction matrix. NKL_{modes} is the same for both DMs, the modal filtering being left to be managed through the inversion process. The KL basis is built for one $r_{0,}$ L_0 couple which is frozen for the whole study. The KL basis is made orthogonal to the previously defined Tip, Tilt and defocus modes, controlled by the LO NGS loop.
- Build $IM_{l2s\text{-}GS}$ of dimension [N_{gs}× N_{slopes}, N_{layers}× NKL_{modes}] with N_{gs}=4 and N_{layers} = 2. This is a virtual modal "MCAO" Interaction Matrix (IM) between the modes generated at N_{layers} different layers and the slopes measured by the N_{gs} LGS WFSs. It is simulated with the PSIM code by setting the following parameters:
    - Misregistrations on each LGS WFS as measured on ASSIST, in Shift X and Y in % of subaperture, rotation in degree and magnification in X and Y in % of pupil:
        - LGS1: [3; -13; 178.72; -0.11; 0.04]
        - LGS2: [-7; -11; 177.88; -0.78; -0.83]
        - LGS3: [-3; -6; 178.49; -1.22; -1.20]
        - LGS4: [4; -19; 178.40; -0.56; -0.76]
    - The FoV diameter: 20" allowing to define the metapupil diameter.
    - The angular positions of the 4 LGS in Alpha Delta
        - Alpha= [-10; 0; 10; 0]
        - Delta= [0; -10; 0; 10]
    - Layer altitudes: ground 0 m and altitude 8.2506 km, where the metapupil has a diameter of 44 subapertures
    - LGS altitude = 90 km
    - Definition of the calibration modes at the ground and in altitude: NKL_{modes} first KL modes per layer

  For the altitude part of $IM_{l2s\text{-}GS,}$ the subapertures with low standard deviation (smaller than 0.6 times the median of the standard deviation of all subapertures) are identified. The signal measured in these subapertures is set to zero in the vDM IM. This methods allows mitigating the vDM edge effects in the metapupil. Of course, other geometrical criteria may be used. The disabled actuators (columns) and subapertures (lines) are removed from the IM before inversion and then incorporated as respectively lines and columns of zeros.
- $CM_{s2l\text{-}GS}$ = [N_{layers}× NKL_{modes}, N_{gs}× N_{slopes}] with N_{gs}=4 and N_{layers} = 2 is the "MCAO" Control Matrix (CM) obtained through inversion of $IM_{l2s\text{-}GS}$. The tomographic process lies in this CM generation. Moreover, since this IM accounts for real features of the 4 LGS WFSs, noise and misregistration in particular, this is where regularization has to be applied. The regularization of the inversion process, described later, is tuned thanks to a "fudge" factor $n_{phot,}$ homogeneous to a number of photons. This is an essential parameter to be scanned and optimized during the system tests, depending on turbulence conditions and measurement signal to noise ratio. Finally, in addition to filtering them out from the modal basis, the projection of the modes Tip/Tilt and Defocus on slopes are removed from the 4 LGS WFS measurements at this stage.
- CM_{dir} is the final LTAO CM obtained by summing the 2 parts of $CM_{s2l\text{-}GS}$ corresponding to the gDM and vDM and then projecting the KL modal basis onto the DSM zonal command basis, via the KL eigenmodes matrix.

4.3 Computation of reconstructor: virtual layer method

The virtual layer method is equivalent to the vDM method but, in addition, provides a sampling of the external metapupils' annuli. Building the reconstructor is also based on a first tomographic step where an "MCAO" CM is generated. The second step, consisting in projecting the various layers on the DSM, is more complex than the simple sum allowed by the vDM method. The main steps to build the virtual layer reconstructor are the following:

- Define a modal basis to calibrate each layer. Two virtual DMs with a square geometry are simulated. The actuator density is equivalent to the DSM's but one of the two DMs has more actuators in order to sample the whole metapupil. The KL bases of each of these two DMs are computed. The first N_{modes} modes are used to calibrate the following interaction matrix. N_{modes} is the same for both DMs, the modal filtering being left to be managed through the inversion process. In this study, $N_{modes} = 1364$. The KL bases are built for one $r_{0,}$ L_0 couple which is frozen for the whole study, assuming an equivalent turbulence energy at the ground and in altitude. The KL bases is made orthogonal to the previously defined Tip, Tilt and defocus modes, controlled by the NGS loop.
- $IM_{l2s\text{-}GS} = [N_{gs} \times N_{slopes}, N_{layers} \times N_{modes}]$ with $N_{gs}=4$ and $N_{layers} = 2$. This is a virtual modal "MCAO" IM built in the same way and assuming identical assumptions as for the vDM method, with the notable exception of not zeroing the subapertures with low standard deviation.
- $CM_{s2l\text{-}GS} = [N_{layers} \times N_{modes}, N_{gs} \times N_{slopes}]$ is the CM obtained through regularized inversion of $IM_{l2s\text{-}GS}$, in the same way as for the vDM.
- $IM_{l2s\text{-}Opt} = [N_{slopes}, N_{layers} \times N_{modes}]$ is an IM between the atmospheric layers and a virtual WFS which can be defined either as:
    - A perfectly registered, centered on axis and noiseless 40x40 WFS looking at an NGS, in order to optimise the science beam on axis. This is the case that we will use to build the virtual layer reconstructor for GALACSI NFM.
    - One of the 4 LGS WFS, with its misregistration, off-axis angle and looking at an LGS at 90 km, in order to minimise the Wave Front Error (WFE) on this particular LGS WFS. This case can allow verifying the tomography performance in absence of a way to measure a PSF or a WFE on axis.
    - A set of several WFSs in the FoV used to optimize the performance across a selected FoV, some kind of LTAO across an extended FoV.
- $P = CM_{s2l\text{-}GS} \cdot IM_{l2s\text{-}Opt} = [N_{slopes}, N_{gs} \times N_{slopes}]$ is the projection matrix that transforms the measurements coming from the 4 LGS WFS into the measurement that would provide a virtual WFS in the direction of interest as defined in $IM_{l2s\text{-}Opt.}$
- $IM_{a2s\text{-}dir} = [N_{slopes}, N_{act}]$ is the IM between a zonal model of the DSM and its N_{act} valid actuators and the virtual WFS defined in $IM_{l2s\text{-}Opt}$
- $CM_{s2a\text{-}dir} = [N_{act}, N_{slopes}]$ is the CM obtained by inversion of $IM_{a2s\text{-}dir}$. The disabled actuators columns are removed from the IM prior to the inversion. Then, the generalized inverse is performed by truncated Singular Value Decomposition (tSVD). A selectable number of DSM KL modes are truncated so that NKL_{modes} will be controlled by the generated reconstructor. Finally, lines with zeros are incorporated into the resulting CM.
- $CM_{dir} = CM_{s2a\text{-}dir} \cdot P = [N_{act}, N_{gs} \times N_{slopes}]$ is the final LTAO CM obtained by multiplying $CM_{s2a\text{-}dir}$ and P.

4.4 "MCAO" IM inversion

A minimum variance reconstruction approach, a.k.a. Minimum Mean Square Error (MMSE), is used to generate the virtual "MCAO" control matrix $CM_{s2l\text{-}GS.}$ Priors on turbulence profile and measurement noise are used to regularize the inversion. However, the open loop priors being applied to closed loop residuals, unlike with the optimal Pseudo Open Loop Control (POLC) scheme [15], a "fudge" factor n_{phot} is used to tune the regularization. The minimum variance inversion can be described by the following equation:

$$CM_{s2l\text{-}GS} = C_u . IM_{l2s\text{-}GS} \left[IM_{l2s\text{-}GS} . C_u . IM_{l2s\text{-}GS}^{\ T} + C_b(n_{phot}) \right]^{-1} \quad (6)$$

Where C_u stands for the covariance matrix of the atmospheric modes. It contains the Prior knowledge on the turbulence spatial statistics expressed in the layers (or vDM) space. Because turbulence is uncorrelated between layers, it is a block matrix, with as many blocks as layers. In our case, 2 layers with identical spatial statistics (same r_0 per layer) are assumed. For C_b, we consider the WFS subapertures as statistically independent with respect to noise. The noise

covariance is then simply a diagonal matrix with the subaperture noise variance on the diagonal. C_b is computed by adding photon noise and detector read-out noise, taking into account the measured subaperture illumination map, the spot size and the "fudge" factor n_{phot}. Measured slopes covariance could as well be used to build the matrix C_b. Finally, the Tip, Tilt and Focus modes (TTF) as defined previously are filtered out from the CM in the following way:

$$CM_{s2l\text{-}GS} = CM_{s2l\text{-}GS} - \left(CM_{s2l\text{-}GS}.TTF^{T}\right)TTF^{-1^{T}} \quad (7)$$

n_{phot} is homogeneous to a number of photons, meaning that the higher n_{phot} the lower the regularization. For an infinite n_{phot}, the inversion tends towards a least square solution (tSVD) without any regularization. Oppositely, the lower n_{phot}, the stronger the regularization, that is to say that more modes are filtered out or controlled with a low modal gain.
A way to evaluate the modal gain vector generated by the regularization process is to plot the diagonal of the matrix $IM_{l2s\text{-}GS}.CM_{s2l\text{-}GS}$. The following figure shows an example illustrating the effect of n_{phot} on the modal gains, the modes being defined as a matrix of KL modes applied only the gDM with zeros on the vDM and vice versa. The gDM and vDM modes appear clearly. As expected, a low n_{phot} induces a damping of the modal gains, proportionally to the spatial order of the concerned mode. On the opposite, a high n_{phot} yields a flattening of the gain vector to a homogeneous value of 1. In this case, all modes are controlled with the same unitary gain in the same way as with a classical least square reconstructor.

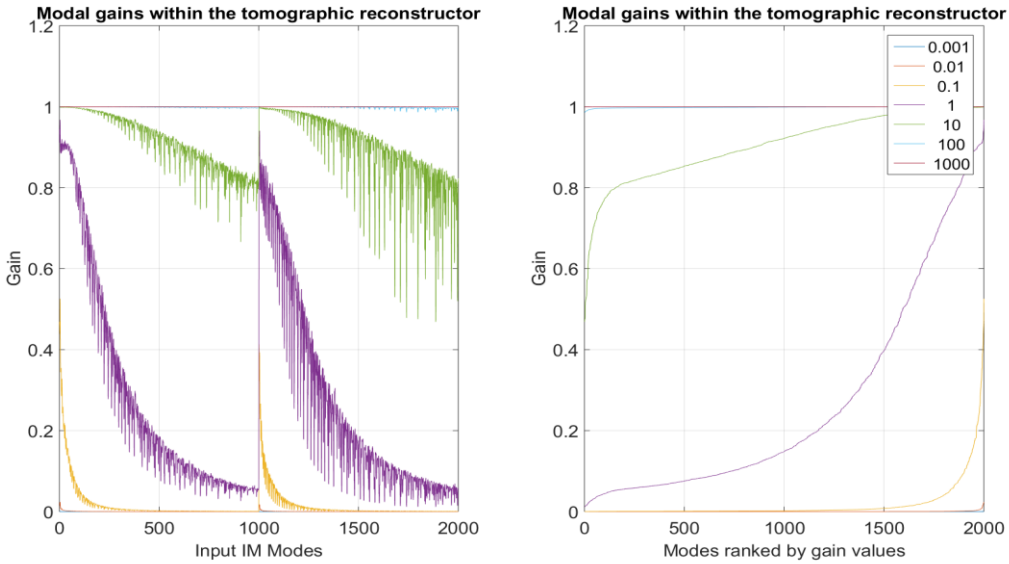

Figure 8: Tomographic modal gains [Left] Gain vs. KL mode number (ground and altitude) [Right] Ranked modal gain value

5. ASSIST TEST BENCH RESULTS AND COMPARISON WITH SIMULATIONS

Based on the approach described in the previous section, tests have been run on the ASSIST bench in order to optimize the tomographic reconstruction and validate the achieved performance.

5.1 High LGS flux – H band performance: regularization vs. turbulence profile

In order to focus on tomography issues, the first tests are performed under a specific configuration offered by an engineering mode turning the LO IR WFS into an H band imager. Basically, the IRLOS' lenslet is removed and replaced by a lens providing a good sampling of the PSF @ 1600 nm with a pixel scale of 9.65 mas. This way, the measured Strehl ratio is higher than in R band and hence allows a better analysis of the trends when scanning parameters.
IRLOS being unusable as LO loop sensor, all modes are controlled by the LGS WFS, including Tip,Tilt and Defocus, which is possible on ASSIST since no LGS uplink jitter is simulated.
Considering the nominal turbulence case for which GALACSI NFM has been specified, i.e. a combination of phase screens types 1, 1 and 2 (PS112), respectively conjugated at 200 m, 5950 m and 9600 m, providing a good integrated seeing of 0.65" with about half of the energy in the ground layer, the best performance is obtained with a virtual layer

reconstructor with n_{phot}=0.8 and $NKL_{modes\sim}$650. In this case, GALACSI NFM achieves a Strehl Ratio (SR) of about 90% relative to the SR obtained without phase screens. Open loop and closed loop linear and log scale PSFs are shown as an example of this operating point on Figure 9.

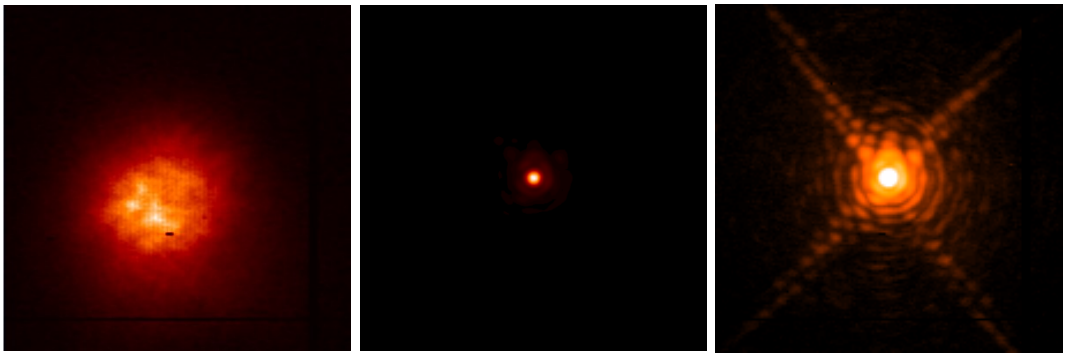

Figure 9: NFM baseline seeing case – 10 s integration – pixel scale: 9.65 mas – FoV: 1.5"
[Left] Open loop PSF [Middle] Closed loop PSF linear scale [Right] Closed loop PSF log scale

Then, we switched between several combinations of phase screens described in Table 1. For each case, the parameters n_{phot} and NKL_{modes} are scanned for both reconstruction approaches: virtual DM and virtual layer.
Figure 10 shows the results in terms of relative performance obtained while scanning the reconstruction parameters. The first conclusion is that the virtual layer approach performs better than the virtual DM. Furthermore, for the two most realistic baseline seeing cases (PS112: NFM and PS311: WFM), it appears that it is not necessary to control more than 600 modes to achieve the best performance for both virtual DM and virtual layer. Moreover, even if many modes can be controlled (we have successfully tested up to 1100), the performance starts dropping when controlling more than 900 modes. However, the case with no high altitude layer (PS310), it is beneficial to control more modes (more than 1000 for the virtual layer). In this case, more regularization is logically required (lower n_{phot} value). An opposite example is the extreme case PS003, where all the turbulence is located at high altitude. There, the best performance is achieved by reducing the regularization because it otherwise penalizes the controllability of altitude mode with higher spatial order.
On Figure 11, for the same turbulence cases as on Figure 10, the relative performance obtained with the virtual DM and virtual layer reconstructors is displayed as function of seeing and isoplanatic angle. The blue and red dashed lines correspond to the best tuning of the reconstruction parameters for each turbulence case while the solid line shows the performance achieved with a constant tuning:

- Virtual DM: n_{phot}=1, NKL_{modes}=600
- Virtual layer: n_{phot}=0.8, $NKL_{modes\sim}$650 (500 truncated modes)

The GLAO performance is plotted as well. Furthermore, simulation dots obtained with ESO's End-to-End AO simulation code Octopus are shown as references [18]. The agreement between measured and simulated performance is remarkable. The trends match the theory in terms of impact of isoplanatic angle and seeing on performance. Moreover, one can observe that the larger the theta0, the more turbulence in the ground layer and hence the closer the performances between GLAO and LTAO.
The GLAO and virtual DM reconstructors' points fit well the simulated results while the virtual layer reconstructor significantly over performs the vDM one. The vDM also exhibits less robustness to misregistrations than the virtual layer reconstructor, which can be explained by edge effects in the metapupil (See § 5.4).Thus, the virtual layer reconstructor is selected as our baseline.
With constant reconstruction tuning, it is interesting to note that even if the performance decreases with respect to the optimal tuning, it remains good and always better than the simulated LTAO performance with the virtual layer reconstructor. Since it is clearly operationally advantageous for robustness reasons to keep a constant reconstructor over such a wide range of atmospheric conditions, we select the virtual layer reconstructor with n_{phot}=0.8 and 500 truncated modes for the bright flux regime. Our baseline strategy is to keep one reconstructor tuning independently of the seeing and C_n^2 profile.

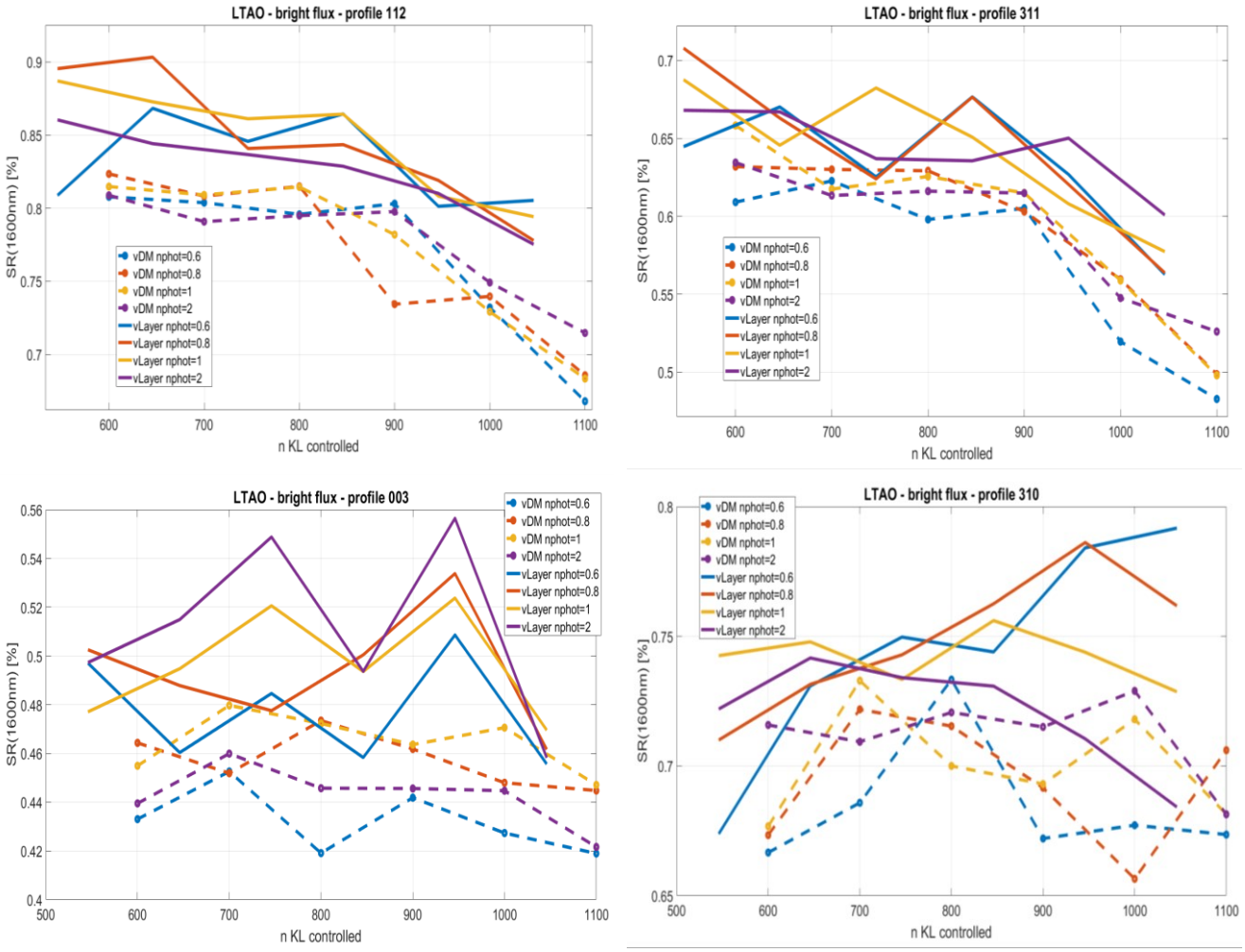

Figure 10: Long exposure (10 s) SR measured @ 1600 nm for different values of n_{phot} and NKL_{modes}. [Top Left] PS112 (baseline NFM case) [Top Right] PS311 (baseline WFM case) [Bottom Left] PS003 [Bottom Right] PS310

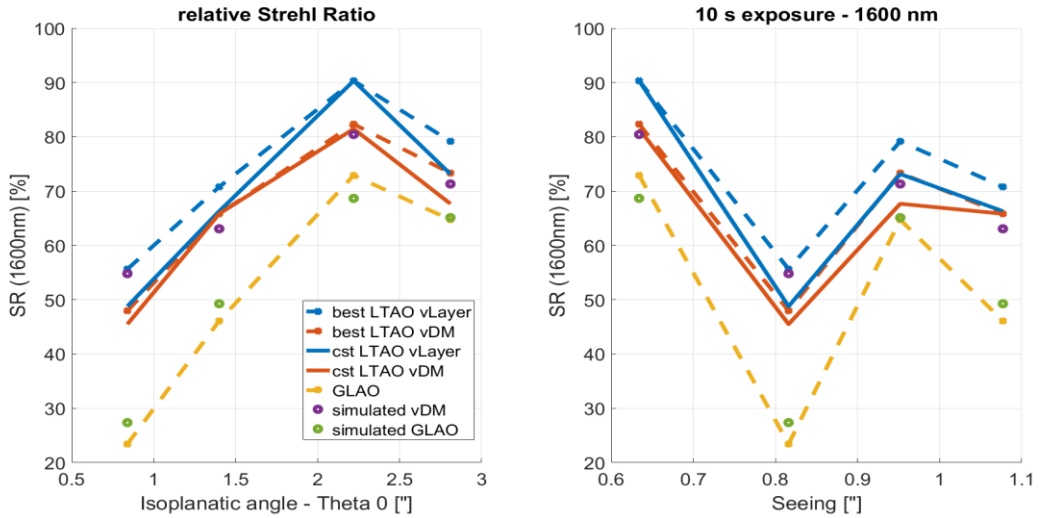

Figure 11: SR @ 1600 nm vs. isoplanatic angle [Left] and Seeing [Right] for LTAO reconstructors and GLAO

5.2 Nominal LGS flux – R band performance: regularization with noise

Using the nominal GALACSI NFM AO mode, controlling Tip, Tilt and Defocus with IRLOS, we investigate here the impact of measurement noise on the reconstructor optimization at nominal LGS flux (88 photons per subaperture per ms). We start from the baseline LTAO reconstructor defined in the previous section, that is to say the virtual layer reconstructor with n_{phot}=0.8 and NKL_{modes} =650. Around this point, the reconstructor main parameters are scanned in the following way:

- For NKL_{modes} =650, nphot=[0.4 0.8 1 2 5]
- For nphot=0.8, the number of truncated KL modes is 1146- NKL_{modes} =[200 300 400 500 600 700 800 900 1000];

At nominal Seeing conditions (PS112), nominal LGS flux of 88 photoelectrons/subaperture/ms and faint NGS (goal magnitude 16) settings, the SR measurements, this time @ 625 nm, shown on Figure 12 confirm that the optimum reconstructor parameters remain the same as the ones found in bright flux regime.

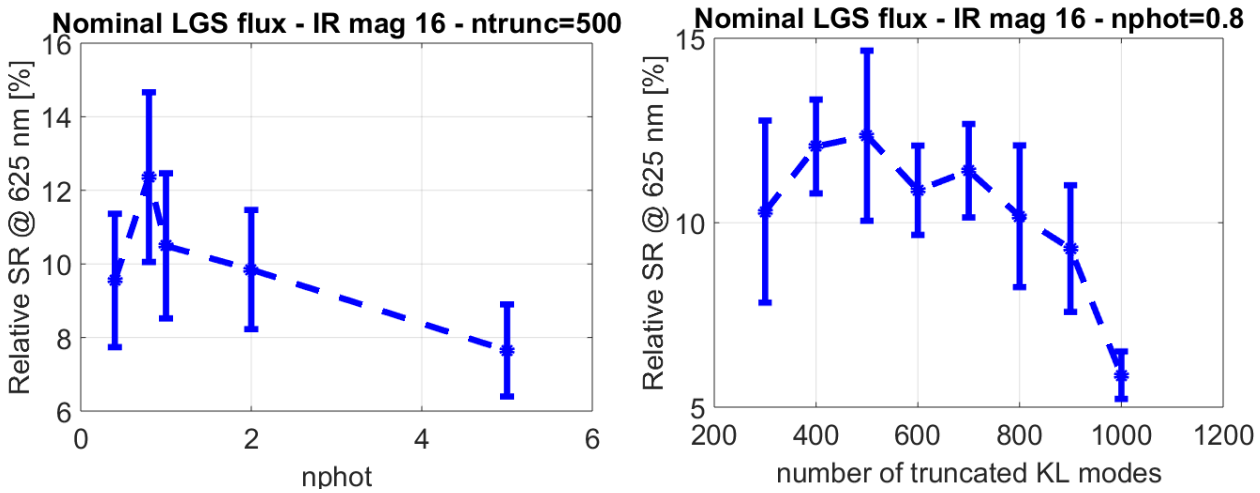

Figure 12: Nominal LGS flux – NGS magnitude 16 - The error bars correspond to +/- 1 rms SR error over 10 exposures of 1s each – [Left] Relative SR @ 625 nm vs. n_{phot} – 500 truncated KL modes [Right] Relative SR @ 625 nm vs. number of truncated modes – nphot=0.8

5.3 Nominal LGS flux – R band performance: Comparison with simulation results for different turbulence profiles

Keeping the same working point as defined in the section above and the baseline reconstructor settings, the sensitivity of performance to seeing and isoplanatic angle is once again investigated. All results are summarized in Table 1. On Figure 14, the measured SRs are displayed in blue against the isoplanatic angle and seeing corresponding to 4 turbulence cases that are most realistic in terms of C_n^2 profile, including the NFM baseline profile (PS112) for which open loop and closed loop visible PSF are shown on Figure 13. The performances simulated by Octopus for the same turbulence cases are displayed in green for an IR NGS of magnitude 15 and in red for an IR NGS of magnitude 16. These two reference curves allow to verify the estimated NGS magnitude of 16, who suffers from uncertainties coming from the bias in flux estimation and the imperfect knowledge of test bench transmission. The main conclusions that can be drawn from this final validation test are the following:

- Once again, the measured performance exhibits a trend which is in good agreement with the simulations. This shows on one hand that the simulations can be trusted and on the other hand that the system performs as expected by design. Performance predictions presented during the Final Design Review of GALACSI demonstrate that GALACSI as-built is in compliance with its major specifications.
- In the NFM nominal turbulence case (0.65” seeing), the relative SR as measured on ASSIST is equal to 12%. Applying to this value a conservative corrective factor 0.64 coming from the NFM error budget (including telescope, instrument and Sodium layer features), the final performance is equal to 7.5%, right between the specification (5%) and its goal (10%). Nevertheless, the final performance will have to be validated during commissioning.

- The loops remain stable over a wide range of turbulence conditions, some of them being considered extreme for such a sensitive LTAO system (faint NGS flux, larger seeing and smaller θ_0). Furthermore, all parameters are frozen when scanning these turbulence cases, especially the LTAO reconstructor which could have been optimized in each case, but we prefer to keep it unchanged for the sake of operational simplicity and in turn robustness and maintainability.
- It is interesting to note that even under worst seeing or anisoplanatism conditions, the loop is stable and no DSM saturation has been witnessed. This shows that a scientific observation will not suffer from seeing bursts.
- The NGS magnitude influences dramatically the performance for magnitude fainter than 15. An upgrade of the Hawaii I detector to SAPHIRA (technology with sub-electron Read-Out Noise [16]) could be considered to improve the performance in limiting magnitude regime.

Figure 13: PSF measured @ 625 nm with the nominal turbulence case (112). [Left] Open loop long exposure [Middle] Closed loop long exposure linear scale [Right] Comparison between Open loop and closed loop PSFs

PS	Remark	Seeing (") θ_0 (")	Cn^2 profile (%) 200 m	5950 m	9600 m	Coherence time τ_0 (ms)	CL SR LTAO 625 nm
311	Nominal WFM	1.077 1.40	63	18.5	18.5	2.8	3.9%
310	Nominal WFM without Altitude layer	0.952 2.81	77.3	22.7	0	3.2	7.4%
003	Study case: all at 9600 m	0.816 0.84	0	0	100	3.2	3.9%
030	Study case: all at 5950 m	0.816 1.36	0	100	0	2.4	5.6%
300	Study case: all at 200 m	0.816 40.42	100	0	0	4.8	13.1%
112	Nominal NFM	0.634 2.22	45	45	10	2.8	11.8%
110	Nominal NFM without Altitude Layer	0.593 2.83	50	50	0	3.4	18%

Table 1: Description of turbulence cases generated by combining 3 phase screens – Measured closed loop SR @ 625 nm for each case, relative to the case without tubulence

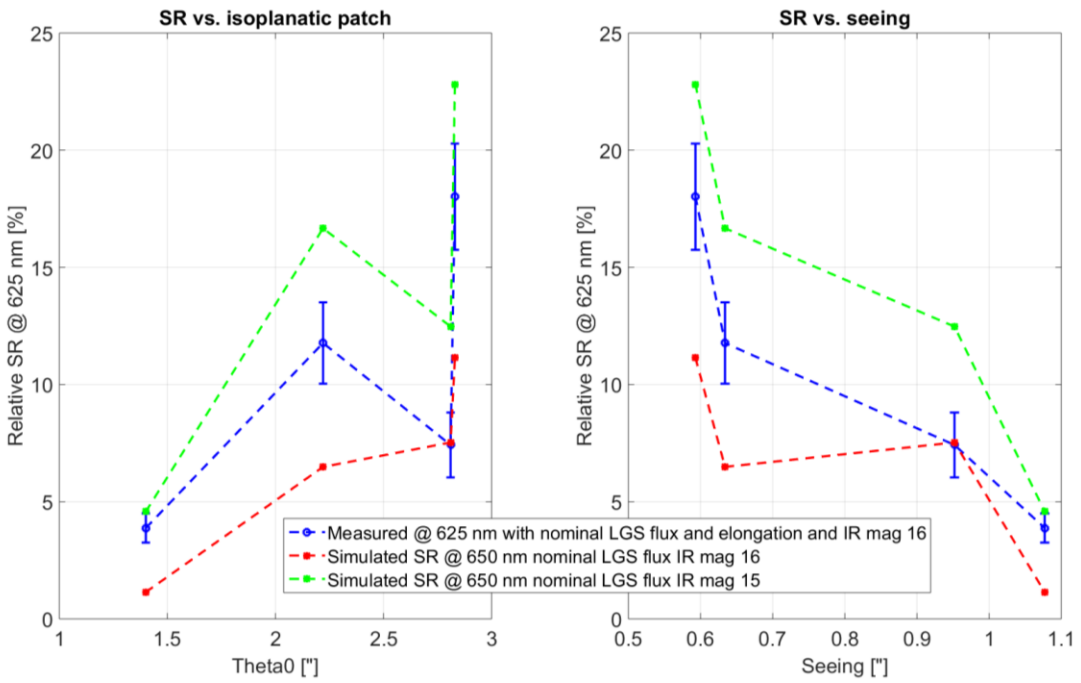

Figure 14: Nominal LGS flux and elongation (short) IR magnitude 16 - SR measured on long exposures @ 625 nm compared to SR simulated @ 650 nm. The error bars stand for +/-1 standard deviation of SR measured on 10 short exposures.

5.4 Impact of mis-registrations on LTAO performance

The sensitivity to mis-registrations is another quality criterion useful to compare different reconstructors. Two methods have been tested to evaluate this sensitivity:

- The alignment (decentering) of ASSIST is not changed, instead the LTAO loop is closed with pseudo-synthetic CMs generated with increasing amounts of pupil shift errors. Two LGS reconstructors controlling all modes are tested (virtual DM and virtual layer). The performance is measured @ 1600nm, then converted @ 625 nm via the Marechal criterion (coherent energy). We see on Figure 15 that the performance is stable until 20% of subaperture size. Then, there is a constant decay until 50% of subaperture, where the loop cannot be closed any longer with the virtual DM reconstructor (or using a large leaky gain). The virtual layer reconstructor exhibits higher robustness and keeps providing good performance at 50% of subaperture, as expected by design thanks to a better management of the edge effects in the metapupil.
- In closed loop with the virtual layer reconstructor, we apply increasing amounts of decentering with the hexapod. The more decentering, the more Coma piles up on the DSM closed loop commands. Our investigation is limited by the stroke of the hexapod in shift, saturating at 38% of subaperture when the Coma stroke represents more than +/- 0.4 SPARTA units. For each hexapod position, the pupil shifts are estimated by means of the flux method, which confirms the design values. The SR is measured @ 625 nm when the loop is closed under two flux conditions, bright LGS + NGS and nominal LGS + IR NGS magnitude 15. The trends shown on Figure 15 exhibit similar behaviours as found with the first method.

Thus, the two main results of this sensitivity study are that:

- The PSIM mimics well the effect of mis-registration and can be used to compensate for it.
- Despite a drop in performance for shifts larger than 20% of subaperture, GALACSI NFM's loop can remain stable until large mis-registrations (> 50% of SA) with the baseline LTAO reconstructor.
- The virtual DM is less robust to mis-registrations.

End-to-end simulations performed with Octopus confirm the low sensitivity of the LTAO mode of GALACSI to DSM shifts. Indeed, Figure 16 confirms that the performance remains stable for shifts smaller than 20 % of subaperture, even

when controlling 1000 modes in the ground layer and 700 modes in the altitude layer. Moreover, these simulations show that reducing the number of controlled modes to 400 in each layer reduces the sensitivity of performance to mis-registrations. GALACSI NFM's baseline being to control 650 modes, we are in an intermediate situation with respect to the simulation cases. This tuning allows us to reach peak performance while keeping a low sensitivity to mis-registrations.

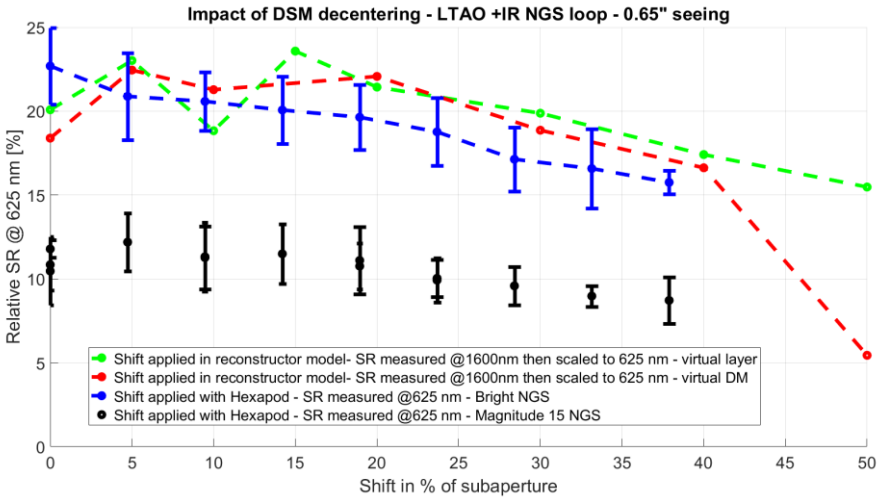

Figure 15: SR @ 625 nm against shift of the DSM in % of subaperture introduced into the reconstructor model [Green and Red] or applied to the Hexapod [Blue and Black]

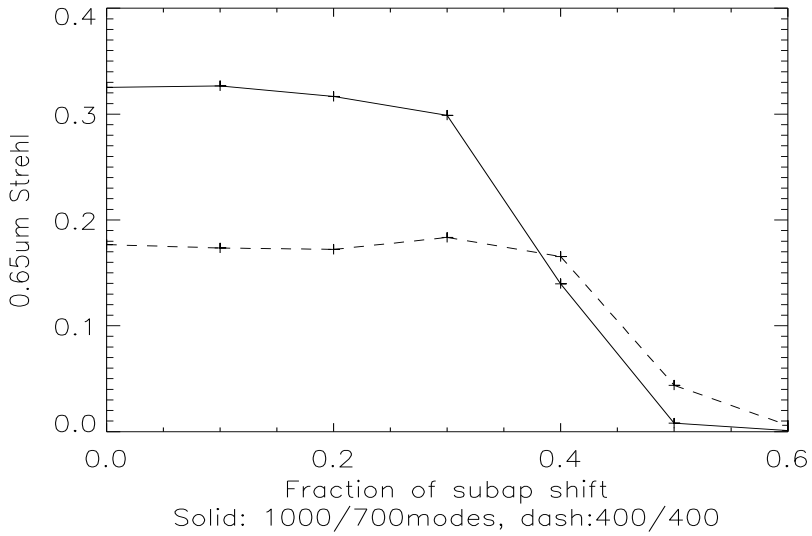

Figure 16: Effect of number of controlled modes on sensitivity to mis-registration. Octopus SR vs. Shift in fraction of subaperture

6. FUTURE WORK

During the GALACSI system tests with ASSIST, the tomographic reconstruction was based on a pseudo-synthetic IM integrating 1 virtual DM (or layer) at 8km altitude. With only three layers in our 3D turbulence simulator, this choice was close to optimal (see Figure 7). Nevertheless, the turbulence profile being continuous in the real world, is this baseline applicable for operations on sky at the VLT?

To prepare the upcoming commissionings, some end-to-end simulations have been run to investigate two aspects with a turbulence profile with 12 layers:

- With one virtual DM, what is the optimal conjugation altitude for different turbulence profiles? For a constant seeing value of 0.8", 3 profiles have been considered:
    - Median: corresponding to the statistical median
    - Good: corresponding to the 25% of the cases with highest ground layer contribution
    - Bad: corresponding to the 25% of the cases with lowest ground layer contribution

  On Figure 17 (left side), the on axis SR is plotted against the altitude of a single vDM for the three turbulence profiles. It shows that the optimal vDM altitude ranges from 14 to 16 km depending on the conditions. Furthermore, the vDM altitude strongly influences the achieved performance. Thus, the virtual layer altitude will have to be tuned differently on sky with respect to our baseline in the lab (8km). Furthermore, even if it seems sufficient to locate it at 15 km regardless from the turbulence profile, this will have to be verified on sky. In particular, we will investigate whether or not it makes sense to optimize the vDM altitude online during the course of an observation, based on real time C_n^2 profile estimation [17].
- What is the influence of the number of vDMs? With a 12 layers turbulence profile @ 0.65" seeing, the number of vDM is scanned between 1 and 10. For each case, the regularization is tuned by scanning $n_{phot.}$ The performance is plotted for each value of $n_{phot.}$ On Figure 17 right side, we plot the SR loss with respect to the performance achieved when reconstructing 10 layers, against the number of vDM. The improvement provided by increasing the number of vDM from 1 to 2 or 3 is moderate. Nevertheless, there is a price to pay in doing so: the more vDM, the harder it is to tune the regularization to ensure stability as exhibited by the spread of regularization points for each vDM number. Thus, one virtual altitude layer remains the baseline for operations at the VLT.

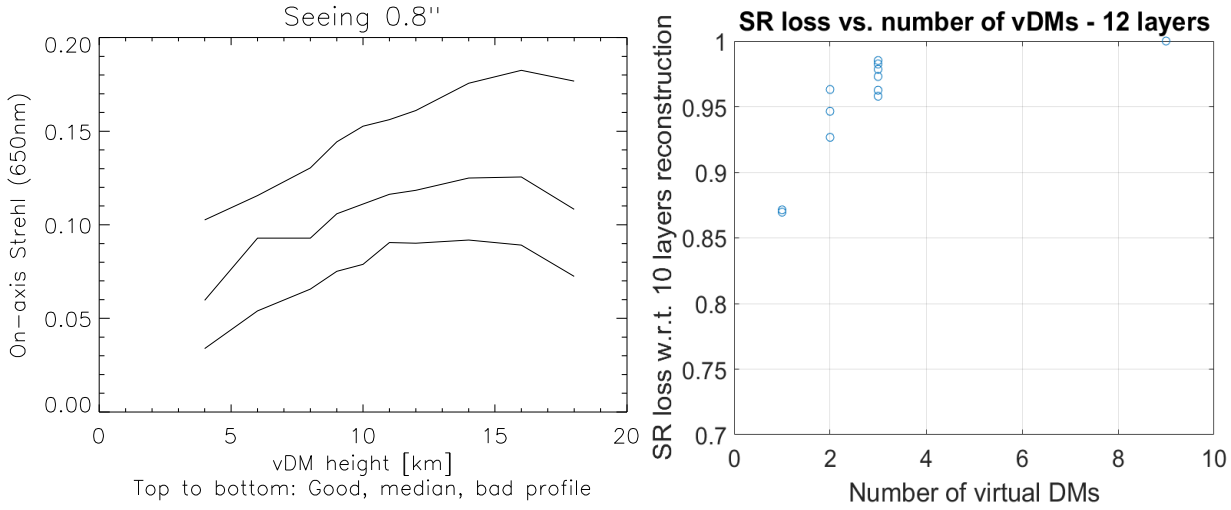

Figure 17: [Left] Impact of a single vDM altitude on performance for 3 turbulence profiles [Right] Impact of number of vDM on performance for GALACSI NFM's baseline turbulence case (seeing=0.65")

The optimization of the altitude of the virtual layer according to online estimation of Cn2 profile estimation will have to be investigated during the commissioning of GALACSI NFM.

Furthermore, the tomographic reconstruction is a major topic for the E-ELT tomographic AO systems, namely MAORY and HARMONI. During the course of the on-going designs studies, several approaches will be investigated. In particular, the optimal POLC [15] reconstruction approach will be considered with care since on the one hand it enables reaching higher performance and robustness but on the other hand induces more stringent requirements on the RTC, which in this case cannot constraint the real time reconstruction to a single MVM like SPARTA does. Moreover, the optimization of the reconstruction with respect to the high resolution real time turbulence profile will probably be a must in the E-ELT case.

7. CONCLUSION

The system tests of GALACSI NFM on the ASSIST test bench have allowed to validate the AOF control strategy based on a pseudo-synthetic tomographic reconstruction. The achieved performance is in line with the simulation results [18] and allows meeting the system specifications. Furthermore, this reconstruction strategy has shown to be robust to turbulence profile evolution as well as mis-registrations. These results will be consolidated on sky during the upcoming commissioning period (Q4 2016 - 2018), during which some additional optimization will be required to account for continuous turbulence profiles. This work will then be extended to the design of E-ELT AO tomographic systems.

REFERENCES

[1] Hackenberg, W. K., Bonaccini Calia, D., Abbad, J. A., Alvarez, J. L., Beltran, J., Buzzoni, B., Comin, M., Del Valle, D., Duhoux, P. R., Dupuy, C., Fischer, G., Gago Rodriguez, F., Guzman, R., Haguenauer, P., Haimerl, P., Holzlöhner, R., Huber, S., Kern, L., van Kesteren, A., Kirchbauer, J. P., Kuntschner, H., Lewis, S., A., Lizon, J.-L., Madec, P.-Y., McLay, S., Munoz, I., Palacio, J. C., Pfrommer, T., Pirard, J.-F., Popovic, D., Quattri, M., Quentin, J., Ridings, R., Riquelme, M., "ESO 4LGSF: Integration in the VLT, Commissioning and on-sky results," Proc. SPIE 9909-27 (2016)

[2] Biasi, R., Andrighettoni, R., Angerer, G., Mair, C., Pescoller, D., Lazzarini, P., Anaclerio, E., Mantegazza, M., Gallieni, D., Vernet, E., Arsenault, R., Madec, P.-Y., Duhoux, P., Riccardi, A., Xompero, M., Briguglio, R., Manetti, M., Morandini, M., "VLT deformable secondary mirror: integration and electromechanical tests results," Proc. SPIE 8447, Adaptive Optics Systems III, 84472G (13 September 2012)

[3] Paufique, J., Madec, P.-Y., Kolb, J., Kuntschner, H., Argomedo, J., Kiekebusch, M. J., Donaldson, R. H., Arsenault, R., Siebenmorgen, R., Soenke, C., Tordo, S., Conzelmann, R. D., Jost, A., Reyes-Moreno, J., Downing, M. D., Valenzuela, J. J., Haguenauer, P., "GRAAL on the mountaintop," Proc. SPIE 9909-91 (2016)

[4] Deep, A., Arsenault, R., Boland, W., Delabre, B., Hubin, N., La Penna, P., Madec, P.-Y., Molster, F., Stuik, R., Tordo, S., Wiegers, E., "Alignment and integration of ASSIST: a test bench for VLT adaptive optics facility," Proc. SPIE 7793, Optical System Alignment, Tolerancing, and Verification IV, 77930L (3 September 2010)

[5] Kolb, J., Madec, P.-Y., Arsenault, R., Oberti, S., Paufique, J., Stroebele, S., Donaldson, R, Soenke, Kiekebusch, M. J., Argomedo, J., Le Louarn, M., Vernet, J. D. R., Haguenauer, P.,Duhoux, P., Valenzuela, J. J., Guerra, J. C., "Laboratory results of the AOF System Testing," Proc. SPIE 9909-105 (2016)

[6] La Penna, P. Stroebele, S., Aller-Carpentier, E., Argomedo, J., Arsenault, R., Conzelmann, R. D., Donaldson, R. H., Gago Rodriguez, F., Gutierrez, P., Hubin, N., Jolley, P. D., Kiekebusch, M. J., Kirchbauer, J. P., Klein, B., Kolb, J., Kuntschner, H., Le Louarn, M., Lizon, J.-L., Madec, P.-Y., Mehrgan, L. H., Oberti, S., Quentin, J., Suárez Valles, M., Soenke, C., Tordo, S., Vernet, J. D. R., "AOF: standalone test results of GALACSI," Proc. SPIE 9909-114 (2016)

[7] Kasper, M., Fedrigo, E., Looze, D.P., Bonnet, H., Ivanescu, L., Oberti, S., "Fast calibration of high-order adaptive optics systems," JOSAA, Opt Image Sci Vis., 21(6):1004-8 (June 2004)

[8] Oberti, S., Quirós-Pacheco, F., Esposito, S., Muradore, R., Arsenault, R., Fedrigo, E., Kasper, M., Kolb, J., Marchetti, E., Riccardi, A., Soenke, C., Stroebele, S., "Large DM AO systems: synthetic IM or calibration on sky?," Proc. SPIE 6272, Advances in Adaptive Optics II, 627220 (28 June 2006)

[9] Esposito, S., Tubbs, R., Puglisi, A., Oberti, S., Tozzi, A., Xompero, M., Zanotti, D., "High SNR measurement of interaction matrix on-sky and in lab," Proc. SPIE 6272, Advances in Adaptive Optics II, 62721C (28 June 2006)

[10] Kolb, J., Madec, P.-Y., Le Louarn, M., Muller, N., Béchet, C., "Calibration strategy of the AOF, "Proc. SPIE 8447, 84472D (2012)

[11] Kolb, J., Martinez, P., Girard, J. H. V., "What can be retrieved from adaptive optics real-time data?,"Proc. SPIE 8447-219 (2012)

[12] Neichel, B. et al., "Gemini multiconjugate adaptive optics system review - II. Commissioning, operation and overall performance," MNRAS, vol. 440, issue 2, p 1002-1019 (May 2014)

[13] Béchet, C., Tallon, M., Thiébaut, E. M., "Optimization of adaptive optics correction during observations: fast algorithms and system parameters identification in closed-loop," Proc. SPIE 8447-84 (2012)

[14] Madec, P.-Y., Kolb, J., Oberti, S., Paufique, J., La Penna, P., Hackenberg, W. K., Kuntschner, H., Argomedo, J., Kiekebusch, M. J., Donaldson, R. H., Suárez Valles, M., Arsenault, R., "Adaptive Optics Facility: control strategy and first on-sky results of the acquisition sequence," Proc SPIE 9909-37 (2016)
[15] Gilles, L., Ellerbroek, Brent L., "Split atmospheric tomography using laser and natural guide stars," JOSAA, vol. 25, issue 10, p. 2427, September 2008
[16] Finger, G. et al., "Development of the near-infrared eAPDarray SAPHIRA achieving sub-electron read noise at millisecond full-frame readout," Proc SPIE 9909-40 (2016)
[17] Neichel, B., Guesalaga, A., Gendron, E., Masciadri, E., Morris, T. J., Fusco, T., Vidal, F., Sivo, G., Osborn, J., Garrel, V., Rousset, G., Rigaut, F., Correia, C. M., Butterley, T., Oberti, S., Kolb, J., Madec, P.-Y., Lardière, O., Conan, J.-M., Robert, C., Ziad, A., Martin, O., Ono, Y. H., "Review on AO real-time turbulence estimation, " Proc. SPIE 9909-16 (2016)
[18] Le Louarn, M., Madec, P.-Y., Kolb, J., Paufique, J., La Penna, P, Arsenault, R., Oberti, S., "Comparison between simulations and lab results on the ASSIST test-bench for the AOF," Proc. SPIE 9909-277 (2016)